University of Zurich[UZH]

Zurich Open Repository and Archive
University of Zurich
University Library
Strickhofstrasse 39
CH-8057 Zurich
www.zora.uzh.ch

Year: 2018

A short BRCA2-derived cell-penetrating peptide targets RAD51 function and confers hypersensitivity towards PARP inhibition

Trenner, Anika ; Godau, Julia ; Sartori, Alessandro A

Abstract: Under conditions of genotoxic stress, cancer cells strongly rely on efficient DNA repair to survive and proliferate. The human BRCA2 tumor suppressor protein is indispensable for the repair of DNA double-strand breaks by homologous recombination (HR) by virtue of its ability to promote RAD51 loading onto single-stranded DNA. Therefore, blocking the interaction between BRCA2 and RAD51 could significantly improve the efficacy of conventional anti-cancer therapies. However, targeting protein-protein interaction (PPI) interfaces has proven challenging because flat and large PPI surfaces generally do not support binding of small molecule inhibitors. In contrast, peptides are more potent for targeting PPIs but are otherwise difficult to deliver into cells. Here, we report that a synthetic 16-mer peptide derived from the BRC4 repeat motif of BRCA2 is capable of blocking RAD51 binding to BRCA2. Efficient non-cytotoxic cellular uptake of a nona-arginine (R9)-conjugated version of the BRC4 peptide interferes with DNA damage-induced RAD51 foci formation and HR. Moreover, transduction of the BRC4 peptide impairs replication fork protective function of BRCA2 and triggers MRE11-dependent degradation of nascent DNA in response to DNA replication stress. Finally, the BRC4 cell-penetrating peptide (CPP) confers selective hypersensitivity to PARP inhibition in cancer cells but spares non-cancerous cells. Taken together, our data highlight an innovative approach to develop novel peptide-based DNA repair inhibitors and establish BRCA2-derived CPPs as promising anti-cancer agents.

DOI: https://doi.org/10.1158/1535-7163.MCT-17-1156

Posted at the Zurich Open Repository and Archive, University of Zurich
ZORA URL: https://doi.org/10.5167/uzh-151663
Journal Article
Accepted Version

Originally published at:
Trenner, Anika; Godau, Julia; Sartori, Alessandro A (2018). A short BRCA2-derived cell-penetrating peptide targets RAD51 function and confers hypersensitivity towards PARP inhibition. Molecular Cancer Therapeutics, 17(7):1392-1404.
DOI: https://doi.org/10.1158/1535-7163.MCT-17-1156

Author Manuscript Published OnlineFirst on April 13, 2018; DOI: 10.1158/1535-7163.MCT-17-1156
Author manuscripts have been peer reviewed and accepted for publication but have not yet been edited.

A short BRCA2-derived cell-penetrating peptide targets RAD51 function and confers hypersensitivity towards PARP inhibition

Anika Trenner[1], Julia Godau[1] and Alessandro A. Sartori[1]

[1]Institute of Molecular Cancer Research, University of Zurich, Winterthurerstrasse 190, CH-8057 Zurich, Switzerland

Running title: A synthetic BRCA2 peptide inhibits RAD51

Corresponding Author: Alessandro A. Sartori, Institute of Molecular Cancer Research, University of Zurich, Winterthurerstrasse 190, CH-8057 Zurich, Switzerland. Phone: +41446353473; Fax: +41446353484; E-mail: sartori@imcr.uzh.ch

Disclosure of Potential Conflicts of Interest: No potential conflicts of interest were disclosed

Downloaded from mct.aacrjournals.org on May 23, 2018. © 2018 American Association for Cancer Research.

Author Manuscript Published OnlineFirst on April 13, 2018; DOI: 10.1158/1535-7163.MCT-17-1156
Author manuscripts have been peer reviewed and accepted for publication but have not yet been edited.

Abstract

Under conditions of genotoxic stress, cancer cells strongly rely on efficient DNA repair to survive and proliferate. The human BRCA2 tumor suppressor protein is indispensable for the repair of DNA double-strand breaks by homologous recombination (HR) by virtue of its ability to promote RAD51 loading onto single-stranded DNA. Therefore, blocking the interaction between BRCA2 and RAD51 could significantly improve the efficacy of conventional anti-cancer therapies. However, targeting protein-protein interaction (PPI) interfaces has proven challenging because flat and large PPI surfaces generally do not support binding of small molecule inhibitors. In contrast, peptides are more potent for targeting PPIs but are otherwise difficult to deliver into cells. Here, we report that a synthetic 16-mer peptide derived from the BRC4 repeat motif of BRCA2 is capable of blocking RAD51 binding to BRCA2. Efficient non-cytotoxic cellular uptake of a nona-arginine (R9)-conjugated version of the BRC4 peptide interferes with DNA damage-induced RAD51 foci formation and HR. Moreover, transduction of the BRC4 peptide impairs replication fork protective function of BRCA2 and triggers MRE11-dependent degradation of nascent DNA in response to DNA replication stress. Finally, the BRC4 cell-penetrating peptide (CPP) confers selective hypersensitivity to PARP inhibition in cancer cells but spares non-cancerous cells. Taken together, our data highlight an innovative approach to develop novel peptide-based DNA repair inhibitors and establish BRCA2-derived CPPs as promising anti-cancer agents.

Downloaded from mct.aacrjournals.org on May 23, 2018. © 2018 American Association for Cancer Research.

Author Manuscript Published OnlineFirst on April 13, 2018; DOI: 10.1158/1535-7163.MCT-17-1156
Author manuscripts have been peer reviewed and accepted for publication but have not yet been edited.

Introduction

Double-strand breaks (DSBs) are highly detrimental DNA lesions because, if left unrepaired or misrepaired, they can trigger cell death and genomic instability, ultimately causing cancer (1). To circumvent this threat, cells are equipped with diverse DSB repair mechanisms including non-homologous end-joining (NHEJ) and homologous recombination (HR) as the two major pathways (2). Furthermore, recent work has established that in response to DNA replication stress several key HR factors play a crucial role in protecting stalled DNA replication forks from nucleolytic degradation (3). Because rapidly dividing cancer cells rely on efficient DSB repair and fork protection mechanisms for their survival, inhibiting HR represents an attractive strategy for the development of novel therapeutic drugs, in particular when used in combination with DNA-damaging agents (4,5).

The human BRCA2 protein plays an essential role in HR by promoting homology search and stimulating strand invasion into the sister chromatid (6). Specifically, following DNA-end resection, BRCA2 directs RAD51 filament nucleation onto RPA-coated single-stranded DNA (ssDNA) (7). RAD51 interacts with two distinct regions in BRCA2, the BRC repeat motifs and a C-terminal domain (8-10). Importantly, the eight evolutionarily conserved BRC repeats, each consisting of about 35 amino acids, significantly differ in their capacity to bind RAD51 with BRC4 displaying the highest affinity (11,12). Consequently, it was proposed that BRC repeats 1-4 facilitate nucleation of RAD51 by binding monomeric RAD51 and reducing its ATPase activity (11,13). Structural analysis of the BRC4 repeat identified residues 1523-GFHTASG-1529 of BRCA2 to structurally mimic the self-oligomerization motif of RAD51 (14). In addition to the FHTA motif, a second consensus tetrameric module in BRC4, denoted as LFDE motif, was shown to bind to a distinct pocket in RAD51

Downloaded from mct.aacrjournals.org on May 23, 2018. © 2018 American Association for Cancer Research.

Author Manuscript Published OnlineFirst on April 13, 2018; DOI: 10.1158/1535-7163.MCT-17-1156
Author manuscripts have been peer reviewed and accepted for publication but have not yet been edited.

distant from the oligomerization interface (15). In contrast to the BRC repeats, the C-terminal domain does not bind monomeric RAD51 but instead stabilizes RAD51 nucleoprotein filaments (9,10). Taken together, compounds that selectively and efficiently block BRCA2-RAD51 interaction could advance into the clinic as *bona fide* HR inhibitors for both monotherapy and add-on therapy with DNA-damaging agents.

The physical nature of protein-protein interaction (PPI) interfaces often renders them unable to support binding of small molecule inhibitors (SMIs). Instead, peptide therapeutics offer an alternative way to target PPIs with key advantages over SMIs, including their direct similarity to protein fragments and the coverage of extensive PPI interfaces (16). However, poor membrane permeability has previously limited their use to extracellular targets (17). Thus, hydrophilic peptides are reliant on a permeation enhancing strategy that facilitates targeting of intracellular molecules (18). Recently, cell-penetrating peptides (CPPs) have been developed to enhance the cellular uptake and nuclear translocation of membrane-impermeable cargo molecules (19). They comprise a highly diverse class of short, primarily cationic peptides that combine a limited cytotoxicity and the ability to mediate receptor-independent transport of cargoes across cell membranes (20). Notably, the nona-arginine (R9) peptide is one of the most potent CPPs, giving a high transduction efficiency combined with low cytotoxicity (21).

Here, we design a cell-penetrating peptide comprised of a 16 amino-acid stretch of the BRCA2 BRC4 repeat able to inhibit BRCA2-RAD51 interaction. Our detailed functional analysis reveals that an R9-fused BRC4 CPP prevents RAD51 loading onto ssDNA, resulting in defective homology-mediated repair of DSBs as well as increased MRE11-dependent degradation of stalled DNA replication forks.

Downloaded from mct.aacrjournals.org on May 23, 2018. © 2018 American Association for Cancer Research.

Author Manuscript Published OnlineFirst on April 13, 2018; DOI: 10.1158/1535-7163.MCT-17-1156
Author manuscripts have been peer reviewed and accepted for publication but have not yet been edited.

Consequently, peptide incubation renders cells hypersensitive to the PARP inhibitor olaparib, providing a potential use for BRCA2-derived peptides in the treatment of certain types of cancer.

Downloaded from mct.aacrjournals.org on May 23, 2018. © 2018 American Association for Cancer Research.

Author Manuscript Published OnlineFirst on April 13, 2018; DOI: 10.1158/1535-7163.MCT-17-1156
Author manuscripts have been peer reviewed and accepted for publication but have not yet been edited.

Materials and Methods

Cell culture

HeLa, U2OS, RPE1, MRC5 (all from ATCC) and HeLa DR-GFP were cultured in Dulbecco's Modified Eagle Medium (DMEM, Gibco) supplemented with 10% Fetal Calf Serum (FCS, Sigma-Aldrich), 100 U/ml penicillin and 100 µg/ml streptomycin (P/S, Life Technologies). PEO1 and PEO4 cells were purchased from the Health Protection Agency Culture Collections (Salisbury, UK) and cultured in RPMI Medium (Gibco) supplemented with 10% FCS, 2 mM sodium pyruvate (Gibco) and P/S. MCF10A cells were purchase from American Type Culture Collection (ATCC, Manassas, VA) and cultured in DMEM/F12 (Gibco) containing 5% Horse Serum (Gibco), 20 ng/ml human EGF (Sigma-Aldrich), 0.5 mg/ml Hydrocortisone (Sigma-Aldrich), 10 µg/ml Insulin and P/S. Stable U2OS cells expressing GFP-RAD51 (22) were grown in DMEM supplemented with 10% Tet-system approved FCS (Sigma-Aldrich) and P/S. To induce GFP-RAD51 expression, cells were treated with 1 µg/ml doxycycline (Dox, Sigma Aldrich) for 24 hours. All cell lines were confirmed to be free of mycoplasma contamination on a regular basis (PCR Mycoplasma Test Kit, AppliChem). Cells were passaged for no longer than 2 months after thawing of early-passage stocks. For cells that have been received from secondary sources no cell line authentication was performed. Irradiation was performed using a Faxitron X-ray machine.

Chemicals and peptides

Camptothecin (CPT), RAD51 inhibitor B02 (23), cycloheximide, hydroxyurea (HU) and mirin (24) were purchased from Sigma-Aldrich. Olaparib (AZD2281) was provided by Selleck Chemicals. Thymidine analogs CIdU, IdU and EdU were

Downloaded from mct.aacrjournals.org on May 23, 2018. © 2018 American Association for Cancer Research.

Author Manuscript Published OnlineFirst on April 13, 2018; DOI: 10.1158/1535-7163.MCT-17-1156
Author manuscripts have been peer reviewed and accepted for publication but have not yet been edited.

purchased from Sigma-Aldrich and Life Technologies, respectively. Custom-designed peptides were purchased from Bachem AG (Bubendorf, Switzerland) and, if not specified, synthesized according to standard practice (L-amino acids, N-terminal tag or acetylation, C-terminal amidation). Lyophilized peptides were dissolved in PBS at 1 mg/ml.

Antibodies

A detailed list of all primary and secondary antibodies can be found in Supplementary Tables 1 and 2, respectively.

siRNA

A detailed list of siRNA oligonucleotide sequences used in this study can be found in Supplementary Table 3. siRNA oligos were used at a final concentration of 10 nM and transfected using Lipofectamine RNAiMAX (Invitrogen) according to manufacturer's instructions.

Recombinant protein expression

BRCA2 GST-fusion plasmids (GST-BRC 1-2, GST-BRC3-5, GST-BRC6-8, GST-C-term) have been described before (25). BRCA2 GST-fusion proteins were expressed in BL21-CodonPlus-RIL *E. coli* by growing them overnight at 18°C using 100 μM isopropyl β-D-thiogalactoside. Recombinant full-length RAD51 was prepared as previously described (26).

Immunoblotting

If not specified otherwise, cells were lysed in Laemmli buffer (4% SDS, 20%

Downloaded from mct.aacrjournals.org on May 23, 2018. © 2018 American Association for Cancer Research.

Author Manuscript Published OnlineFirst on April 13, 2018; DOI: 10.1158/1535-7163.MCT-17-1156
Author manuscripts have been peer reviewed and accepted for publication but have not yet been edited.

glycerol, 120 mM Tris-HCl pH 6.8) and resolved by Tris-glycine SDS-PAGE. In order to probe for BRCA2, 3-6% NuPAGE Tris-Acetate gels (ThermoFisher) were run according to manufacture's instructions. After transfer to nitrocellulose membranes, immunoblotting was performed with indicated primary antibodies overnight at 4°C and secondary antibodies for 1 hour at room temperature. Stained proteins were visualized using the Advansta WesternBright ECL reagent and the VilberLourmat Fusion Solo S imaging system**.**

Pull-down assays

For peptide pull-downs, 30 µl streptavidin-coupled Dynabeads (Life Technologies) were incubated with 5 µg (2.7 nmol) of biotinylated BRC4 peptides or biotin analogue d-Desthiobiotin (Sigma-Aldrich) in 1 ml PBS-T (0.1% Triton X-100) for 1 hour at 4°C. Beads were washed three times with PBS-T and blocked for 30 min with 0.3% BSA in PBS at 4°C. 50 ng (1.35 pmol) recombinant RAD51 together with 2 µM ATP was added to the beads and incubated for 2 hours in 700 µl PBS-T. The beads were washed four times with NTEN300 (20 mM Tris pH 7.4, 0.1 mM EDTA, 300 mM NaCl, 0.5% NP-40) and once with TEN100 (20 mM Tris pH 7.4, 0.1 mM EDTA, 100 mM NaCl) before complexes were boiled in 5x SDS sample buffer (25 mM Tris pH 6.8, 50% glycerol, 8% SDS, 500 mM DTT, 0.1% Bromphenol blue) and subjected to immunoblotting. For GST pull-down assays, glutathione sepharose beads (GE Healthcare) were incubated for 1 hour at 4°C with equalized amounts of BL21 *E. coli* soluble extracts expressing one of the four GST-BRCA2 fusion constructs in TEN100. Beads were washed three times with NTEN300 buffer and once with TEN100 before adding either 1 mg HeLa nuclear extracts (CilBiotech, Mons, Belgium) or 50 ng purified RAD51 supplemented with varying amounts of $BRC4^{wt}$ or

Downloaded from mct.aacrjournals.org on May 23, 2018. © 2018 American Association for Cancer Research.

Author Manuscript Published OnlineFirst on April 13, 2018; DOI: 10.1158/1535-7163.MCT-17-1156
Author manuscripts have been peer reviewed and accepted for publication but have not yet been edited.

BRC4^{mut} peptides filled up to 1 ml with TEN100. After 2 hours of incubation, beads were washed twice with NTEN500 (20 mM Tris pH 7.4, 0.1 mM EDTA, 500 mM NaCl, 0.5% NP-40), twice with NTEN300 and twice with TEN100 buffer before boiling in SDS sample buffer and protein analysis by immunoblotting.

Co-immunoprecipitation

Cell extracts were prepared using NP-40 extraction buffer (50 mM Tris-HCl pH 7.5, 120 mM NaCl, 1 mM EDTA, 6 mM EGTA, 15 mM sodium pyrophosphate and 1% NP-40 supplemented with phosphatase inhibitors (20 mM NaF, 1 mM sodium orthovanadate) and protease inhibitors (1 mM benzamidine and 0.1 mM PMSF)). After Benzonase (Novagen) digestion for 30 min at 4°C, cell extracts were cleared by centrifugation. 2 mg of lysates were supplemented with increasing amounts of peptides filled up to 1 ml with NP-40 extraction buffer and incubated for 1 hour at 4°C before adding 20 µl GFP-Trap agarose beads (ChromoTek) for 1 hour at 4°C. Beads were subsequently washed three times with GFP-IP buffer (100 mM NaCl, 0.2% NP-40, 1 mM $MgCl_2$, 10% glycerol, 5 mM NaF, 50 mM Tris-HCl pH 7.5) and boiled in SDS sample buffer for analysis by immunoblotting.

Peptide transfection

Cells were seeded either into 8-well chamber imaging slides (µ-Slide 8 Well, ibidi), 24-well plates, 6-well plates, or 6 cm culture dishes (Sarstedt) and grown to around 80% confluence at day of peptide transfection. Cells were washed at least once with PBS to remove residual FCS and incubated with indicated peptide concentrations in appropriate serum-free medium for 1 hour at 37°C. If not specified otherwise, the following incubation volumes were used: 0.3 ml for eight-well chamber imaging

Downloaded from mct.aacrjournals.org on May 23, 2018. © 2018 American Association for Cancer Research.

Author Manuscript Published OnlineFirst on April 13, 2018; DOI: 10.1158/1535-7163.MCT-17-1156
Author manuscripts have been peer reviewed and accepted for publication but have not yet been edited.

slides and 24-well plates, 0.5 ml for 12-well plates and 2 ml for 6-well plates and 6 cm culture dishes.

Confocal microscopy

40'000 cells were seeded into eight-well chamber imaging slides and grown overnight. After a 30 minutes staining with 0.5 µg/ml Hoechst 33342 (Life Technologies), cells were washed twice with PBS and incubated with indicated peptide concentrations. Cells were washed twice with PBS and imaged in Live Cell Imaging solution (ThermoFisher). Images were taken with CLSM SP5 Mid UV-VIS Leica with 63x objective at 37°C at ambient CO_2 concentrations.

Flow cytometry

EdU incorporation was analyzed using the Click-it EdU technology (ThermoFisher) according to manufacturer's instructions. For peptide uptake studies, 100'000 cells were seeded into 12-well plates. The day after, peptide transfection was performed and cells were harvested by trypsinization to remove membrane-bound peptides. After one wash with PBS, cells were resuspended in PBS and subjected to flow cytometry analysis. To quantify intracellular peptide stability, same cells were released for indicated time points in DMEM + 10% FCS and fixed with 4% formaldeyhde (w/v) in PBS for 15 minutes at room temperature. To measure the TAMRA fluorescence intensity, the LSR II Fortessa equipped with a 561 nm laser line and a 586/15 band-pass filter was used. Of note, the fluorescence intensity of TAMRA-labeled R9-BRC4^{mut} peptides was corrected for quenching by multiplying measured TAMRA intensity with a quenching factor. The quenching factor was calculated by loading 10 pmol of freshly solubilized peptides on Tricine SDS-PAGE gel and quantifying

Downloaded from mct.aacrjournals.org on May 23, 2018. © 2018 American Association for Cancer Research.

Author Manuscript Published OnlineFirst on April 13, 2018; DOI: 10.1158/1535-7163.MCT-17-1156
Author manuscripts have been peer reviewed and accepted for publication but have not yet been edited.

TAMRA intensity (see Figure 2C, lane 5). Fluorescein intensity was measured with Attune Nxt Flow Cytometer equipped with 488 laser and 530/30 band-pass filter. For each condition 20'000 events were recorded. MACS Quant® Calibration Beads (MACS Miltenyi Biotec) were applied for voltage standardization in order to exclude any machine-dependent variations between measurements.

Tricine SDS-PAGE

To resolve low molecular weight peptides, Tricine SDS-PAGE was performed as described previously (27). For peptide separation, Laemmli lysates were loaded onto 16% Tricine SDS-PAGE gel containing 6 M urea. For peptide detection via fluorescence, gels were scanned using a Typhoon FLA 9500 FluorImager.

HR reporter assay

HR frequency was measured as described previously (28,29). Briefly, following siRNA transfection, 100'000 HeLa cells containing a stably integrated DR-GFP reporter construct were seeded into 12-well plates. The day after, cells were either mock-transfected or transfected with 0.6 µg *I-SceI* expression plasmid (pCBASce) using jetPrime transfection reagent (Polyplus transfection). 4 hours later medium was exchanged and either a one-hour peptide incubation or second siRNA transfection was performed. Peptide incubations were repeated 24 and 34 hours post-*I-SceI* transfection. After each peptide incubation, 0.5 ml of DMEM + 20% FCS was directly added to the peptide/DMEM mix. 48 hours after *I-SceI* transfection, cells were harvested and directly analyzed for GFP expression by flow cytometry using an Attune Nxt Flow Cytometer.

Downloaded from mct.aacrjournals.org on May 23, 2018. © 2018 American Association for Cancer Research.

Author Manuscript Published OnlineFirst on April 13, 2018; DOI: 10.1158/1535-7163.MCT-17-1156
Author manuscripts have been peer reviewed and accepted for publication but have not yet been edited.

Immunofluorescence microscopy

24 hours post-siRNA transfection, 80'000 cells were seeded on coverslips in 24-well plates. The day after, cells were treated either with 100 nM CPT for 1 hour or irradiated and incubated for another hour with the peptides, before releasing them for 3 hours by directly adding 1 ml of DMEM + 14% FCS. Alternatively, cells were transfected with the peptides, followed by 1-hour CPT treatment and direct processing. Cells were pre-extracted for 5 minutes on ice (25 mM HEPES pH 7.4, 50 mM NaCl, 1 mM EDTA, 3 mM $MgCl_2$, 300 mM sucrose, 0.5% Triton X-100), fixed with 4% formaldeyhde (w/v) in PBS for 15 minutes at room temperature, before incubating them with indicated primary and appropriate secondary antibodies for 1 hour. Afterwards, coverslips were mounted with Vectashield (Vector Laboratories) containing DAPI and sealed. Images were acquired on Leica DMI6000 widefield fluorescence microscope with a 63x objective.

DNA fiber analysis

DNA fiber analyses were carried out as described previously (30). In brief, U2OS cells were seeded into 6-well plates at a confluence of 40%. 24 hours later, cells were pulse-labeled with 33 μM CIdU for 30 minutes, followed by 340 μM IdU for 30 minutes prior to incubation with 2 mM HU and peptides (10 μM) for 4 hours in serum-free medium. Cells were lysed (200 mM Tris-HCl pH 7.4, 50 mM EDTA, 0.5% SDS) and DNA fibers were stretched onto glass slides before fixation in Methanol-Acetic acid (3:1, Merck) overnight. Rehydration in PBS was followed by denaturation in 2.5 M HCl for 1 hour, a PBS wash and blockage (2% BSA (w/v) PBS, 0.1% Tween 20) for 40 minutes. CIdU and IdU staining was performed using anti-BrdU primary and secondary antibodies for 2.5 hours. Coverslips were mounted using

Downloaded from mct.aacrjournals.org on May 23, 2018. © 2018 American Association for Cancer Research.

Author Manuscript Published OnlineFirst on April 13, 2018; DOI: 10.1158/1535-7163.MCT-17-1156
Author manuscripts have been peer reviewed and accepted for publication but have not yet been edited.

Antifade Gold (Invitrogen). Images were acquired on Olympus microscope IX81 with 60x magnification and analysis was carried out using ImageJ software.

Colony-formation assay

Indicated cell lines were plated in poly-L-lysine (Sigma-Aldrich) coated 24-well plates at low cell dilutions of 200 cells/well in technical triplicates. PEO1 and PEO4 cells were seeded at 500 and 1000 cells/well, respectively. 24 hours later, cells were washed once with PBS and incubated with olaparib in presence or absence of peptides. After 1 hour, 1 ml of appropriate medium containing 14% FCS with indicated olaparib concentrations was directly added to the cells without removing the peptide solution. For MCF10A cells, FCS concentration of culture medium was increased to 7%. Alternatively, HeLa cells were treated for 1 hour with 1 μM CPT, washed twice with PBS and peptide transfection was carried out for 1 hour before directly adding 1 ml of DMEM + 14% FCS. Cells were grown for 10 days before fixation with crystal violet solution (0.5 % crystal violet, 20% ethanol (w/v)). For analysis, plates were scanned and analyzed with the ImageJ Plugin ColonyArea using the parameter Colony Intensity, integrating the percentage of the covered area and staining intensity (31).

Statistical analysis

All results were confirmed in at least two independent experiments. Quantitative data are displayed as mean ± s.d. and statistical analyses were performed using GraphPad Prism 7. P values < 0.05 were considered significant.

Downloaded from mct.aacrjournals.org on May 23, 2018. © 2018 American Association for Cancer Research.

Author Manuscript Published OnlineFirst on April 13, 2018; DOI: 10.1158/1535-7163.MCT-17-1156
Author manuscripts have been peer reviewed and accepted for publication but have not yet been edited.

Results

BRC4 peptide inhibits BRCA2-RAD51 interaction.

It is well established that BRCA2 binds RAD51 through its BRC repeats composed of two highly conserved tetrameric motifs (Supplementary Fig. S1A). Among the eight BRC repeats, BRC4 was reported to display the highest affinity for RAD51, mainly using its FHTA sequence to bind the RAD51 oligomerization motif. To specifically target the BRCA2-RAD51 protein interaction interface, we therefore synthesized a 16-mer peptide mimicking the N-terminal half of BRC4 comprising the FHTA hydrophobic motif (Fig. 1A). In addition to the 'wild type' BRC4 peptide ($BRC4^{wt}$), we included a 'mutated' BRC4 peptide ($BRC4^{mut}$) harboring an inverted FHTA sequence (Fig. 1A). Employing N-terminally biotinylated peptides, recombinant RAD51 was efficiently pulled down by $BRC4^{wt}$ but to a much lesser extent by $BRC4^{mut}$ (Fig. 1B). In agreement with previous reports (32), we observed that GST-tagged BRCA2 fusion proteins spanning BRC 1-2, BRC 3-5 or the C-terminal (C-term) domain were able to interact with RAD51 (Supplementary Fig. S1B and Fig. 1C). Remarkably, $BRC4^{wt}$ was able to outcompete each of these individual interactions in a concentration-dependent manner (Fig. 1D). Interestingly, the BRC4 peptide was more effective in outcompeting RAD51 binding to the BRCA2 C-term and BRC repeats 1-2 than to BRC repeats 3-5 (Fig. 1D), indicating that the BRC4 repeat of BRCA2 exhibits the highest binding affinity for RAD51. Similar GST pull-down results were obtained using HeLa nuclear extracts as a source for RAD51 (Supplementary Fig. S1C). Given that the BRCA2 C-terminal region exclusively binds to assembled RAD51 oligomers, we reasoned that the BRC4 peptide is able to disrupt RAD51 multimers present in solution, which is in agreement with binding of the FHTA cluster to the RAD51 oligomerization motif (9,10,14). Most importantly,

Downloaded from mct.aacrjournals.org on May 23, 2018. © 2018 American Association for Cancer Research.

Author Manuscript Published OnlineFirst on April 13, 2018; DOI: 10.1158/1535-7163.MCT-17-1156
Author manuscripts have been peer reviewed and accepted for publication but have not yet been edited.

co-immunoprecipitation experiments in U2OS cells inducibly expressing GFP-tagged RAD51 demonstrated that $BRC4^{wt}$, but not $BRC4^{mut}$, is capable of interfering both with BRCA2 binding to RAD51 and RAD51 oligomerization (Fig. 1E and Supplementary Figs. S1D and S1E). Taken together, our results indicated that a short, synthetic BRC4-derived peptide is proficient in blocking BRCA2-RAD51 protein-protein interaction.

The cell-penetrating peptide R9 facilitates intracellular delivery of BRC4.

Native peptides do not readily cross cell membranes. To enhance cellular uptake, we decided to conjugate BRC4 peptides with a nona-arginine (R9) cell-penetrating peptide (CPP). Additionally, a red fluorescent dye (TAMRA) was N-terminally attached to R9-BRC4 peptides to analyze cellular uptake. Using confocal microscopy, we observed robust cytoplasmic and nuclear TAMRA signals in HeLa and U2OS cells upon transfection with R9-fused peptides (Fig. 2A). Moreover, we found that the concentration threshold for efficient R9-BRC4 cell penetration was above 10 μM (Supplementary Fig. S2A). Flow cytometry analyses further confirmed that BRC4 peptide delivery reached a transduction efficiency of almost 100% when fused to R9 (Fig. 2B and Supplementary Fig. S2B). Importantly, when replacing the TAMRA label with a green fluorescent dye (Fluorescein), we observed very similar subcellular localization patterns and fluorescent intensities of the R9-BRC4 peptides (Supplementary Figs. S2C and S2D). As peptides are prone to proteolytic degradation upon cellular uptake, we next determined the amount of intact peptides being delivered to the cells. In order to differentiate between full-length and degraded peptides, whole-cell lysates of HeLa and U2OS cells incubated with fluorescently labeled peptides were subjected to SDS-PAGE designed for resolving very low

Downloaded from mct.aacrjournals.org on May 23, 2018. © 2018 American Association for Cancer Research.

Author Manuscript Published OnlineFirst on April 13, 2018; DOI: 10.1158/1535-7163.MCT-17-1156
Author manuscripts have been peer reviewed and accepted for publication but have not yet been edited.

molecular weight protein species (27). Using this approach, we detected significant amounts of intact TAMRA- and Fluorescein-labeled R9-BRC4 peptides being effectively delivered to HeLa and U2OS cells (Fig. 2C and Supplementary Fig. S2E). Comparing the band intensity of TAMRA signals between 10 pmol of freshly solubilized peptides directly loaded onto the gel and those of peptide-transduced cell lysates, we calculated a delivery rate of approximately 10^7 peptides per cell, yielding an estimated intracellular peptide concentration of around 1-10 µM (Fig. 2C).

Next, to more precisely determine the intracellular residence time and stability of our BRC4 CPPs, we modified a previously established method (33) and monitored the Fluorescein signal intensity in HeLa cells over a time course of 24 hours after peptide incubation. SDS-PAGE analysis revealed that $BRC4^{wt}$ as well as $BRC4^{mut}$ cargo peptides were gradually degraded with an approximate half-life of 2 hours (Fig. 3A). Strikingly, using the same experimental set up, flow cytometry analysis of Fluorescein-R9-$BRC4^{wt}$ indicated a rather heterogeneous degradation pattern, which was most pronounced after 8 hours with a large proportion of cells still showing moderate to high fluorescent intensities (Fig. 3B).

Collectively, we concluded that intracellular uptake of R9-$BRC4^{wt}$ and R9-$BRC4^{mut}$ was efficient and comparable as determined by confocal microscopy, flow cytometry and SDS-PAGE analysis, thus providing a solid basis for further mechanistic investigations.

BRC4 peptide specifically inhibits RAD51-mediated homologous recombination.

Conditional overexpression of full-length BRC4 was previously shown to inhibit DNA damage-induced RAD51 foci formation in MCF7 (breast cancer) and chicken DT40 cells (12,34). Therefore, we wanted to investigate whether the 16-mer BRC4

Downloaded from mct.aacrjournals.org on May 23, 2018. © 2018 American Association for Cancer Research.

Author Manuscript Published OnlineFirst on April 13, 2018; DOI: 10.1158/1535-7163.MCT-17-1156
Author manuscripts have been peer reviewed and accepted for publication but have not yet been edited.

peptide fused to R9 was able to mimic this phenotype, indicative of effective disruption of RAD51 binding to BRCA2. To this end, HeLa or U2OS cells were first incubated with our peptides and subsequently treated with the DNA topoisomerase I poison camptothecin (CPT) to induce replication-dependent DSBs. Importantly, we did not detect any significant change in CPT-induced ATM and CHK2 phosphorylation as well as γH2AX foci formation upon peptide addition, indicating regular activation of apical DNA damage response kinases (Fig. 4A and Supplementary Figs. S3A and S3B). In contrast, CPT-induced RAD51 foci formation in both cell lines was specifically compromised in presence of $BRC4^{wt}$ but not $BRC4^{mut}$ CPPs (Figs. 4B and 4C and Supplementary Figs. S3C and S3D). In line with this observation, $BRC4^{wt}$ significantly suppressed RAD51 foci formation following ionizing radiation (Fig. 4D). Notably, intrinsic RAD51 protein stability was not affected by $BRC4^{wt}$ cellular uptake (Supplementary Fig. S3E). To directly examine the impact of BRC4 peptides on DSB repair by HR, we performed repair reporter assays (DR-GFP) in HeLa cells and observed a significant decrease in HR frequency upon repetitive $BRC4^{wt}$ transfections (Fig. 4E). Throughout all experiments reported in this section, we observed that siRNA-mediated BRCA2 depletion conferred much stronger phenotypes compared to delivery of the $BRC4^{wt}$ peptide.

In summary, our findings suggested that delivery of a synthetic BRC4 peptide potently inhibits RAD51 foci formation and HR, most likely as a result of defective BRCA2-mediated RAD51 loading onto resected DSBs.

BRC4 peptide causes MRE11-dependent degradation of stalled replication forks.

BRCA2-dependent RAD51 loading is not only critical for HR, but has also been established to protect stalled replication forks from nucleolytic degradation by

Downloaded from mct.aacrjournals.org on May 23, 2018. © 2018 American Association for Cancer Research.

Author Manuscript Published OnlineFirst on April 13, 2018; DOI: 10.1158/1535-7163.MCT-17-1156
Author manuscripts have been peer reviewed and accepted for publication but have not yet been edited.

MRE11 (35,36). Thus, we examined a potential effect of the BRC4 peptide on replication fork protection by performing dual-labeling DNA fiber assays in the presence of hydroxyurea (HU), which stalls fork progression. Strikingly, we found that the BRC4^{wt} CPP resulted in shortening of nascent DNA tracts, indicative of increased fork degradation (Fig. 5A). BRC4 intracellular uptake did not interfere with global replication rates, as we could not observe any differences in EdU incorporation (Supplementary Fig. S4). Similar to what has been shown for BRCA2-deficient cells, fork degradation in BRC4 peptide-transduced cells was completely rescued both by mirin, an MRE11 small molecule inhibitor (Fig. 5B), and by siRNA-mediated MRE11 depletion (Fig. 5C). Of note, BRC4 delivery did not result in additive or synergistic effects when delivered into BRCA2-depleted cells, indicating that peptide-mediated fork degradation resulted most likely from specific targeting of the BRCA2-RAD51 interaction (Fig. 5C).

BRC4 peptide confers hypersensitivity to PARP inhibition in cancer cell lines.

Based on our molecular analyses providing robust evidence of the inhibitory effect of the BRC4 peptide on BRCA2 functions in HR and fork protection, we next sought to determine if it also sensitizes cells to DNA-damaging agents. Profound hypersensitivity of BRCA2 mutant cells to poly(ADP-ribose) polymerase (PARP) inhibitors has become an emerging therapeutic paradigm known as synthetic lethality (37). Therefore, we performed clonogenic survival assays in peptide-transfected HeLa cells treated with the PARP inhibitor olaparib (38). Indeed, targeting of the BRCA2-RAD51 interaction by BRC4^{wt} CPPs resulted in a significant reduction in cellular viability in response to chronic PARP inhibition (Figs. 6A and 6B). Consistent with impaired RAD51 foci formation, delivery of BRC4^{wt} CPPs also sensitized HeLa cells

Downloaded from mct.aacrjournals.org on May 23, 2018. © 2018 American Association for Cancer Research.

Author Manuscript Published OnlineFirst on April 13, 2018; DOI: 10.1158/1535-7163.MCT-17-1156
Author manuscripts have been peer reviewed and accepted for publication but have not yet been edited.

to CPT (Supplementary Fig. S5A). Upon treatment with olaparib, we estimated the IC50 value of BRC4 to be around 10 μM for HeLa cells (Fig. 6C). Importantly, R9-BRC4^{wt} alone did not decrease cell survival in otherwise undamaged cells (Fig. 6C). Moreover, despite its relatively short half-life, the efficacy of BRC4 CPPs in sensitizing HeLa cells to PARP inhibition was comparable to that of the B02 small-molecule compound, which specifically inhibits RAD51 binding to DNA (23,39) (Fig. 6D). To further exclude potential off-target effects of the BRC4 CPP in stimulating olaparib-induced cytotoxicity, we employed PEO1 (BRCA2 null) and PEO4 (BRCA2 revertant to wild-type) isogenic ovarian cancer cell lines (40). Notably, we observed a strong synergy between PARP inhibition and R9-BRC4 peptides in PEO4 cells, whereas PEO1 cells did not exhibit BRC4-mediated sensitivity towards olaparib (Supplementary Fig. S5B). Differential peptide uptake could be excluded as both cell lines displayed comparable uptake efficiency and intracellular peptide localization (Supplementary Fig. S5B). Finally, in addition to HeLa cells, we observed that BRC4 CPPs elicited olaparib-induced cell death of U2OS human osteosarcoma cells but not of non-cancerous cell lines, including hTERT-immortalized human retinal pigment epithelial cells (hTERT-RPE1), SV40-immortalized human fetal lung fibroblasts (MRC5) and human breast epithelial cells (MCF10A) (Fig. 6E and Supplementary Fig. S6A). This finding could at least in part be explained by an overall low cellular uptake efficiency and predominant endosome trapping of BRC4 peptides in RPE1, MRC5 and MCF10A non-tumorigenic cell lines (Supplementary Figs. S6B and S6C).

Downloaded from mct.aacrjournals.org on May 23, 2018. © 2018 American Association for Cancer Research.

Author Manuscript Published OnlineFirst on April 13, 2018; DOI: 10.1158/1535-7163.MCT-17-1156
Author manuscripts have been peer reviewed and accepted for publication but have not yet been edited.

Discussion

PPIs represent attractive but at the same time challenging targets for pharmacological intervention in cancer therapy. The emergence of successful peptide-based PPI inhibitors seemed promising, yet drug development was faced with the low membrane translocation ability of native peptides. The identification of a wide range of carrier molecules, commonly termed as CPPs or protein transduction domains, provided a possible solution for this major limitation (19).

Here, we designed a 16-amino acid short peptide derived from the N-terminal half of the human BRCA2 BRC4 repeat able to occupy the RAD51 oligomerization interface and thereby potently inhibiting the interaction between BRCA2 and RAD51. Covalent fusion of the BRC4 peptide with the cationic polyarginine R9 CPP resulted in efficient uptake into both cytoplasm and nucleus, causing defects in HR repair, increased fork degradation, and, ultimately, hypersensitivity to DNA-damaging agents.

Detailed biochemical studies have demonstrated that the full-length BRC4 repeat covering both FHTA and LFDE tetrameric cluster motifs selectively interacts with RAD51 and inhibits RAD51-DNA complex formation (15,41). In order to increase the likelihood of intracellular peptide uptake (42), we reduced the length of the native BRC4 peptide sequence from 35 to 16 amino acids, including only the first FHTA module, which was shown to mimic the RAD51 oligomerization motif (14). In line with our findings, a similar 17-mer N-terminal BRC4 peptide was reported to compete with full-length BRC4 for RAD51 binding, albeit with modest potency (15). We further corroborated the importance of the FHTA sequence by showing that BRC4 16-mer peptides harboring a mirrored ATHF sequence display greatly reduced RAD51 binding affinity.

Downloaded from mct.aacrjournals.org on May 23, 2018. © 2018 American Association for Cancer Research.

Author Manuscript Published OnlineFirst on April 13, 2018; DOI: 10.1158/1535-7163.MCT-17-1156
Author manuscripts have been peer reviewed and accepted for publication but have not yet been edited.

Importantly, intracellular BRC4 peptide uptake in the low micromolar range was sufficient to impair BRCA2-RAD51 complex formation. A high uptake efficiency was likely achieved through a combination of the potent CPP R9 with the beneficial biochemical properties of the BRC4 peptide, including its positive net charge, hydrophobicity, and three-dimensional conformation (18). CPP internalization involves both endocytosis and direct translocation, whereby direct cell penetration is preferred because endocytosis can lead to the trapping of peptides in endosomes and their ultimate degradation (18). Multiple factors, including the CPP, cargo identity, concentration, cell type and differentiation status, influence the balance between both uptake mechanisms (18). We primarily observed a diffuse fluorescent staining and only minor punctuate patterns, indicative of direct translocation as the preferred uptake mechanism. The substantial number of peptide molecules reaching the intracellular space might compensate for the short half-life. Even though only 5% of intact peptides are present 24 hours after transfection, the absolute peptide number per cell at this stage still adds up to 10^6 functional peptides. According to a recent proteomics study in the U2OS cell line, most proteins involved in DSB repair processes including BRCA2 were shown to be of low to moderate abundance (10^2-10^4 copies per cell) (43). Based on these numbers, we speculated that BRC4 peptides are present in high molar excess over their endogenous BRCA2 target protein even 24 hours after uptake.

RAD51 and its property to self-assemble are under dynamic control to enable faithful homology-directed DSB repair. Yu *et al.* proposed the presence of three RAD51 fractions in the cell: a mobile fraction of RAD51 monomers, an immobile oligomerized fraction, and an immobile BRCA2-bound fraction (44). Strikingly, they found the BRCA2-bound fraction to be selectively mobilized upon DNA damage and

Downloaded from mct.aacrjournals.org on May 23, 2018. © 2018 American Association for Cancer Research.

Author Manuscript Published OnlineFirst on April 13, 2018; DOI: 10.1158/1535-7163.MCT-17-1156
Author manuscripts have been peer reviewed and accepted for publication but have not yet been edited.

suggested a dual BRCA2 function of RAD51 sequestration and mobilization. Importantly, the other fractions did not change, suggesting that only the BRCA2-bound RAD51 fraction is involved in DNA repair. Notably, R9-BRC4^{wt} did not affect viability under unstressed growth conditions of conventionally cultured cancer cell lines. Thus, we hypothesize that under normal, undamaged conditions, RAD51 is stably bound to BRCA2 and the peptide's affinity for RAD51 is not high enough to disassemble the protein complex. Accordingly, the BRC4 mimetic peptide is only able to disassemble mobilized BRCA2-RAD51 complexes. We speculate that upon mobilization and ultimate RAD51 loading onto ssDNA, the protein complex becomes increasingly unstable due to an equilibrium change during DNA loading. In this context, the peptide is potent enough to sequester RAD51 transiently dissociated from BRCA2. We further presume that at low levels of DNA damage, requiring only a small fraction of BRCA2-bound RAD51, repair processes are not significantly disturbed by the BRC4 peptide. However, upon increasing DNA damage load and replication stress, when there is a high demand of functional BRCA2-RAD51 complexes, a major pool of RAD51 is sequestered away from BRCA2 by the BRC4 peptide.

Despite its potentially rather high dissociation constant compared to SMIs, BRC4 peptides provided an unexpectedly high degree of specificity. CPPs have often been reported to cause unspecific membrane disruption, which has led to false conclusions regarding their specificity for a number of peptide therapeutics. Since we do not observe a decrease in cell viability upon BRC4 peptide uptake, we can exclude such unspecific CPP-mediated toxicity (45). Furthermore, our finding that MRE11 depletion fully rescued the peptide-induced replication fork degradation phenotype and the lack of synergy between peptides and PARP inhibition in BRCA2-deficient

Downloaded from mct.aacrjournals.org on May 23, 2018. © 2018 American Association for Cancer Research.

Author Manuscript Published OnlineFirst on April 13, 2018; DOI: 10.1158/1535-7163.MCT-17-1156
Author manuscripts have been peer reviewed and accepted for publication but have not yet been edited.

cancer cells argue against potential off-target activity of the BRC4 CPP. Nevertheless, when comparing the outcomes of siRNA-mediated BRCA2 depletion *versus* R9-BRC4^{wt} peptide delivery, depletion is commonly yielding much more pronounced phenotypes. A possible explanation for this relates to the high susceptibility of peptides to extra- and intracellular protease attacks (17). To improve their pharmacokinetic potential, possible peptide optimizations include various backbone modifications and cyclization (17,46). Moreover, the BRCA2-RAD51 interaction might not be completely abolished by the BRC4 peptide as it only comprises the first FHTA but lacks the second LFDE tetrameric cluster motif.

The lack of cell-type specificity is commonly reported to present another major limitation of CPP-mediated drug delivery (19,20). Strikingly, we could not find a synergistic relationship between the PARP inhibitor olaparib and the R9-BRC4 peptide in normal cell lines as compared to cancer cell lines. Interestingly, our peptide uptake data suggest an overall decreased intracellular BRC4 concentration. It is reasonable to speculate that efficient intracellular peptide delivery relies on specific membrane components or lipid compositions that are more uptake responsive in cancer *versus* non-cancerous cell lines. Numerous reports classify lipid metabolic reprogramming as a major source of cell transformation (47). Specifically, the sphingolipid metabolism, which was suggested to influence R9-mediated peptide uptake, was reported to significantly alter during transformation (48). Additionally, cancer cells possess a more negatively charged membrane than normal cells, which is partly caused by a loss in membrane symmetry and the exposure of anionic phosphatidylcholine on the outer leaflet (49). This feature, in combination with higher membrane fluidity (50), might favor the uptake of the cationic R9-BRC4 peptide.

Ultimately, the BRC4 peptide could emerge as a potent radio- and chemosensitizer.

Downloaded from mct.aacrjournals.org on May 23, 2018. © 2018 American Association for Cancer Research.

Author Manuscript Published OnlineFirst on April 13, 2018; DOI: 10.1158/1535-7163.MCT-17-1156
Author manuscripts have been peer reviewed and accepted for publication but have not yet been edited.

Specifically, BRC4 peptide-induced HR-deficiency could represent a promising strategy for expanding the utility of PARP inhibitors, successfully applied in breast and ovarian cancer patients with a germline BRCA1 or BRCA2 mutation (51,52), to BRCA-proficient cancers. Similarly, the BRC4 peptide could re-sensitize BRCA1/2-mutated tumors that acquired chemoresistance to PARP inhibitors by restoring HR (53). Moreover, malignant cells are frequently compromised in genome stability maintenance pathways that are synthetically lethal with HR deficiency (54). Consequently, monotherapy with the identified BRCA2 peptide inhibitor could provide a promising option for the treatment of these tumors. The BRCA2-BRC4 peptide described in this study could also be applied in combination with proton irradiation, which was shown to be highly advantageous over conventional photon therapy. Notably, it was found that HR-deficient tumor cells exhibit an enhanced susceptibility towards proton- versus photon irradiation (55). Drug-induced HR-deficiency with the BRC4 peptide inhibitor could make this advantageous effect accessible for patients with HR-proficient tumors. Lastly, we reveal a straightforward approach to study distinct PPIs in a biological context without the need of elaborate mutagenesis methodologies and provide a potent research tool to study BRCA2-dependent RAD51 loading to ssDNA in different biological contexts.

Downloaded from mct.aacrjournals.org on May 23, 2018. © 2018 American Association for Cancer Research.

Author Manuscript Published OnlineFirst on April 13, 2018; DOI: 10.1158/1535-7163.MCT-17-1156
Author manuscripts have been peer reviewed and accepted for publication but have not yet been edited.

Acknowledgments

The authors would like to thank Roland Brock (Institute of Molecular Life Sciences, Radboud University Nijmengen, Netherlands), Martin Pruschy (Clinic of Radiation Oncology, University Hospital Zurich, Switzerland) and Stefano Ferrari (Institute of Molecular Cancer Research, University of Zurich, Switzerland) for scientific input. We are grateful to Pavel Janscak (Institute of Molecular Cancer Research, University of Zurich, Switzerland) for providing purified, recombinant RAD51 protein and anti-RAD51 rabbit polyclonal antibody and to Fumiko Esashi (Sir William Dunn School of Pathology, University of Oxford, UK) for providing the GST-tagged BRCA2 fusion plasmids. Furthermore, we are grateful to Ross Chapman (Nuffield Department of Medicine, University of Oxford, UK) for providing hTERT-RPE1 cells, Minoru Takata (Radiation Biology Center, Kyoto University, Japan) for the U2OS GFP-RAD51 cell line, Marcel van Vugt (Medical Oncology Department, University Medical Centre Groningen, Netherlands) for HeLa DR-GFP cells and Steve Jackson (Gurdon Institute, Cambridge, UK) for MRC5 cells. We also want to thank Antonio Porro (Institute of Molecular Cancer Research, University of Zurich, Switzerland) for critical reading of the manuscript. This study was supported by research grants from the Krebsliga Schweiz (KFS-3845-02-2016, to A. A. Sartori), Swiss National Science Foundation (31003A_156023 and 31003A_176161, to A. A. Sartori), Promedica Stiftung (1317/M to A. A. Sartori) and Novartis Foundation for Medical-Biological Research (#17C155 to A. A. Sartori).

Downloaded from mct.aacrjournals.org on May 23, 2018. © 2018 American Association for Cancer Research.

Author Manuscript Published OnlineFirst on April 13, 2018; DOI: 10.1158/1535-7163.MCT-17-1156
Author manuscripts have been peer reviewed and accepted for publication but have not yet been edited.

References

1. Negrini S, Gorgoulis VG, Halazonetis TD. Genomic instability--an evolving hallmark of cancer. Nat Rev Mol Cell Biol. 2010 ed. 2010;11:220–8.

2. Ceccaldi R, Rondinelli B, D'Andrea AD. Repair Pathway Choices and Consequences at the Double-Strand Break. Trends in Cell Biology. 2016;26:52–64.

3. Kolinjivadi AM, Sannino V, de Antoni A, Técher H, Baldi G, Costanzo V. Moonlighting at replication forks - a new life for homologous recombination proteins BRCA1, BRCA2 and RAD51. FEBS Lett. 2017;591:1083–100.

4. Hühn D, Bolck HA, Sartori AA. Targeting DNA double-strand break signalling and repair: recent advances in cancer therapy. Swiss Med Wkly. 2013;143:w13837.

5. Carvalho JFS, Kanaar R. Targeting homologous recombination-mediated DNA repair in cancer. Expert Opin Ther Targets. 2014;18:427–58.

6. Fradet-Turcotte A, Sitz J, Grapton D, Orthwein A. BRCA2 functions: from DNA repair to replication fork stabilization. Endocr Relat Cancer. 2016;23:T1–T17.

7. Liu J, Doty T, Gibson B, Heyer W-D. Human BRCA2 protein promotes RAD51 filament formation on RPA-covered single-stranded DNA. Nat Struct Mol Biol. 2010;17:1260–2.

8. Wong AK, Pero R, Ormonde PA, Tavtigian SV, Bartel PL. RAD51 interacts with the evolutionarily conserved BRC motifs in the human breast cancer susceptibility gene brca2. J Biol Chem. 1997;272:31941–4.

9. Esashi F, Galkin VE, Yu X, Egelman EH, West SC. Stabilization of RAD51 nucleoprotein filaments by the C-terminal region of BRCA2. Nat Struct Mol Biol. 2007;14:468–74.

10. Davies OR, Pellegrini L. Interaction with the BRCA2 C terminus protects RAD51-DNA filaments from disassembly by BRC repeats. Nat Struct Mol Biol. 2007;14:475–83.

11. Carreira A, Kowalczykowski SC. Two classes of BRC repeats in BRCA2 promote RAD51 nucleoprotein filament function by distinct mechanisms. Proc Natl Acad Sci USA. 2011;108:10448–53.

12. Chen CF, Chen PL, Zhong Q, Sharp ZD, Lee WH. Expression of BRC repeats in breast cancer cells disrupts the BRCA2-Rad51 complex and leads to radiation hypersensitivity and loss of G(2)/M checkpoint control. J Biol Chem. 1999;274:32931–5.

13. Carreira A, Hilario J, Amitani I, Baskin RJ, Shivji MKK, Venkitaraman AR, et al. The BRC Repeats of BRCA2 Modulate the DNA-Binding Selectivity of RAD51. Cell. 2009;136:1032–43.

Downloaded from mct.aacrjournals.org on May 23, 2018. © 2018 American Association for Cancer Research.

Author Manuscript Published OnlineFirst on April 13, 2018; DOI: 10.1158/1535-7163.MCT-17-1156
Author manuscripts have been peer reviewed and accepted for publication but have not yet been edited.

14. Pellegrini L, Yu DS, Lo T, Anand S, Lee M, Blundell TL, et al. Insights into DNA recombination from the structure of a RAD51-BRCA2 complex. Nature. 2002;420:287–93.

15. Rajendra E, Venkitaraman AR. Two modules in the BRC repeats of BRCA2 mediate structural and functional interactions with the RAD51 recombinase. Nucleic Acids Res. 2009;38:82–96.

16. Ivanov AA, Khuri FR, Fu H. Targeting protein-protein interactions as an anticancer strategy. Trends Pharmacol Sci. 2013;34:393–400.

17. Tsomaia N. Peptide therapeutics: Targeting the undruggable space. Eur J Med Chem. 2015;94:459–70.

18. Kristensen M, Birch D, Mørck Nielsen H. Applications and Challenges for Use of Cell-Penetrating Peptides as Delivery Vectors for Peptide and Protein Cargos. Int J Mol Sci. 2016;17:185–17.

19. Guidotti G, Brambilla L, Rossi D. Cell-Penetrating Peptides: From Basic Research to Clinics. Trends Pharmacol Sci. 2017;38:406–24.

20. Raucher D, Ryu JS. Cell-penetrating peptides: strategies for anticancer treatment. Trends Mol Med. 2015;21:560–70.

21. Tünnemann G, Ter-Avetisyan G, Martin RM, Stöckl M, Herrmann A, Cardoso MC. Live-cell analysis of cell penetration ability and toxicity of oligo-arginines. J Pept Sci. 2008;14:469–76.

22. Sato K, Shimomuki M, Katsuki Y, Takahashi D, Kobayashi W, Ishiai M, et al. FANCI-FANCD2 stabilizes the RAD51-DNA complex by binding RAD51 and protects the 5′-DNA end. Nucleic Acids Res. 2016;44:10758–71.

23. Huang F, Motlekar NA, Burgwin CM, Napper AD, Diamond SL, Mazin AV. Identification of specific inhibitors of human RAD51 recombinase using high-throughput screening. ACS Chem Biol. 2011;6:628–35.

24. Dupré A, Boyer-Chatenet L, Sattler RM, Modi AP, Lee J-H, Nicolette ML, et al. A forward chemical genetic screen reveals an inhibitor of the Mre11-Rad50-Nbs1 complex. Nat Chem Biol. 2008;4:119–25.

25. Lee M, Daniels MJ, Venkitaraman AR. Phosphorylation of BRCA2 by the Polo-like kinase Plk1 is regulated by DNA damage and mitotic progression. Oncogene. 2003;23:865–72.

26. Piwko W, Mlejnkova LJ, Mutreja K, Ranjha L, Stafa D, Smirnov A, et al. The MMS22L-TONSL heterodimer directly promotes RAD51-dependent recombination upon replication stress. The EMBO Journal. 2016;35:2584–601.

27. Schägger H. Tricine-SDS-PAGE. Nat Protoc. 2006;1:16–22.

28. Steger Martin, Murina O, Hühn D, Ferretti LP, Walser R, Hänggi K, et al. Prolyl Isomerase PIN1 Regulates DNA Double-Strand Break Repair by

Downloaded from mct.aacrjournals.org on May 23, 2018. © 2018 American Association for Cancer Research.

Author Manuscript Published OnlineFirst on April 13, 2018; DOI: 10.1158/1535-7163.MCT-17-1156
Author manuscripts have been peer reviewed and accepted for publication but have not yet been edited.

Counteracting DNA End Resection. Mol Cell. 2013;50:333–43.

29. Krajewska M, Fehrmann RSN, Schoonen PM, Labib S, de Vries EGE, Franke L, et al. ATR inhibition preferentially targets homologous recombination-deficient tumor cells. Oncogene. 2015;34:3474–81.

30. Merrick CJ, Jackson D, Diffley JFX. Visualization of altered replication dynamics after DNA damage in human cells. J Biol Chem. 2004;279:20067–75.

31. Guzmán C, Bagga M, Kaur A, Westermarck J, Abankwa D. ColonyArea: An ImageJ Plugin to Automatically Quantify Colony Formation in Clonogenic Assays. PLoS ONE. 2014;9:e92444–9.

32. Esashi F, Christ N, Gannon J, Liu Y, Hunt T, Jasin M, et al. CDK-dependent phosphorylation of BRCA2 as a regulatory mechanism for recombinational repair. Nature. 2005;434:598-604.

33. Ruttekolk IR, Witsenburg JJ, Glauner H, Bovee-Geurts PHM, Ferro ES, Verdurmen WPR, et al. The Intracellular Pharmacokinetics of Terminally Capped Peptides. Mol Pharm. 2012;9:1077-86.

34. Abe T, Branzei D. High levels of BRC4 induced by a Tet-On 3G system suppress DNA repair and impair cell proliferation in vertebrate cells. DNA Repair (Amst). 2014;22:153–64.

35. Schlacher K, Christ N, Siaud N, Egashira A, Wu H, Jasin M. Double-strand break repair-independent role for BRCA2 in blocking stalled replication fork degradation by MRE11. Cell. 2011;145:529–42.

36. Hashimoto Y, Ray Chaudhuri A, Lopes M, Costanzo V. Rad51 protects nascent DNA from Mre11-dependent degradation and promotes continuous DNA synthesis. Nat Struct Mol Biol. 2010;17:1305–11.

37. Farmer H, McCabe N, Lord CJ, Tutt ANJ, Johnson DA, Richardson TB, et al. Targeting the DNA repair defect in BRCA mutant cells as a therapeutic strategy. Nature. 2005;434:917–21.

38. Menear KA, Adcock C, Boulter R, Cockcroft X-L, Copsey L, Cranston A, et al. 4-[3-(4-cyclopropanecarbonylpiperazine-1-carbonyl)-4-fluorobenzyl]-2H-phthalazin-1-one: a novel bioavailable inhibitor of poly(ADP-ribose) polymerase-1. J Med Chem. 2008;51:6581–91.

39. Huang F, Mazina OM, Zentner IJ, Cocklin S, Mazin AV. Inhibition of homologous recombination in human cells by targeting RAD51 recombinase. J Med Chem. 2012;55:3011–20.

40. Sakai W, Swisher EM, Jacquemont C, Chandramohan KV, Couch FJ, Langdon SP, et al. Functional restoration of BRCA2 protein by secondary BRCA2 mutations in BRCA2-mutated ovarian carcinoma. Cancer Res. 2009;69:6381–6.

Downloaded from mct.aacrjournals.org on May 23, 2018. © 2018 American Association for Cancer Research.

Author Manuscript Published OnlineFirst on April 13, 2018; DOI: 10.1158/1535-7163.MCT-17-1156
Author manuscripts have been peer reviewed and accepted for publication but have not yet been edited.

41. Davies AA, Masson JY, McIlwraith MJ, Stasiak AZ, Stasiak A, Venkitaraman AR, et al. Role of BRCA2 in control of the RAD51 recombination and DNA repair protein. Mol Cell. 2001;7:273–82.

42. Renukuntla J, Vadlapudi AD, Patel A, Boddu SHS, Mitra AK. Approaches for enhancing oral bioavailability of peptides and proteins. Int J Pharm. 2013;447:75–93.

43. Beck M, Schmidt A, Malmstroem J, Claassen M, Ori A, Szymborska A, et al. The quantitative proteome of a human cell line. Mol Syst Biol. 2011;7:549.

44. Yu DS, Sonoda E, Takeda S, Huang CLH, Pellegrini L, Blundell TL, et al. Dynamic Control of Rad51 Recombinase by Self-Association and Interaction with BRCA2. Mol Cell. 2003;12:1029–41.

45. El-Andaloussi S, Järver P, Johansson HJ, Langel Ü. Cargo-dependent cytotoxicity and delivery efficacy of cell-penetrating peptides: a comparative study. Biochemical Journal. 2007;407:285–92.

46. Wójcik P, Berlicki Ł. Peptide-based inhibitors of protein-protein interactions. Bioorganic & Medicinal Chemistry Letters. 2016;26:707–13.

47. Beloribi-Djefaflia S, Vasseur S, Guillaumond F. Lipid metabolic reprogramming in cancer cells. Oncogenesis. 2016;5:e189–9.

48. Verdurmen WPR, Thanos M, Ruttekolk IR, Gulbins E, Brock R. Cationic cell-penetrating peptides induce ceramide formation via acid sphingomyelinase: implications for uptake. J Control Release. 2010;147:171–9.

49. Jobin M-L, Bonnafous P, Temsamani H, Dole F, Grélard A, Dufourc EJ, et al. The enhanced membrane interaction and perturbation of a cell penetrating peptide in the presence of anionic lipids: toward an understanding of its selectivity for cancer cells. Biochim Biophys Acta. 2013;1828:1457–70.

50. Sok M, Sentjurc M, Schara M, Stare J, Rott T. Cell membrane fluidity and prognosis of lung cancer. Ann Thorac Surg. 2002;73:1567–71.

51. Fong PC, Boss DS, Yap TA, Tutt A, Wu P, Mergui-Roelvink M, et al. Inhibition of poly(ADP-ribose) polymerase in tumors from BRCA mutation carriers. N Engl J Med. 2009;361:123–34.

52. Robson M, Im S-A, Senkus E, Xu B, Domchek SM, Masuda N, et al. Olaparib for Metastatic Breast Cancer in Patients with a Germline BRCA Mutation. N Engl J Med. 2017;377:523–33.

53. Lord CJ, Ashworth A. Mechanisms of resistance to therapies targeting BRCA-mutant cancers. Nat Med. 2013;19:1381–8.

54. Chernikova SB, Game JC, Brown JM. Inhibiting homologous recombination for cancer therapy. Cancer Biol Ther. 2012;13:61–8.

55. Fontana AO, Augsburger MA, Grosse N, Guckenberger M, Lomax AJ, Sartori

Downloaded from mct.aacrjournals.org on May 23, 2018. © 2018 American Association for Cancer Research.

Author Manuscript Published OnlineFirst on April 13, 2018; DOI: 10.1158/1535-7163.MCT-17-1156
Author manuscripts have been peer reviewed and accepted for publication but have not yet been edited.

AA, et al. Differential DNA repair pathway choice in cancer cells after proton- and photon-irradiation. Radiother Oncol. 2015;116:374–80.

Downloaded from mct.aacrjournals.org on May 23, 2018. © 2018 American Association for Cancer Research.

Author Manuscript Published OnlineFirst on April 13, 2018; DOI: 10.1158/1535-7163.MCT-17-1156
Author manuscripts have been peer reviewed and accepted for publication but have not yet been edited.

Figure Legends

Figure 1. A short BRC4 peptide inhibits BRCA2-RAD51 interaction.

A, Amino acid sequences of BRCA2-derived 16-mer peptides used in this study. In addition to the wild type BRC4 peptide ($BRC4^{wt}$), a mutant version ($BRC4^{mut}$) was included, characterized by an inverted FHTA tetrapeptide motif. **B,** Biotinylated BRC4 peptides coupled to streptavidin beads were used to perform pull-down assays using bacterially expressed and purified human RAD51. Inputs and pulled-down protein complexes were analyzed by immunoblotting. SE and LE denote short and long exposure times of the same anti-RAD51 immunoblot. **C,** Different GST-BRCA2 fusion proteins coupled to glutathione-sepharose beads were used to perform pull-down assays using recombinant RAD51. Inputs and pulled-down protein complexes were analyzed by immunoblotting. **D,** GST-BRCA2 pull-down assays with recombinant RAD51 in the absence or presence of increasing amounts of $BRC4^{wt}$ peptides. Inputs and pulled-down protein complexes were analyzed by immunoblotting. **E,** Lysates of U2OS cells inducibly expressing GFP-RAD51 were supplemented with 50 µg of the indicated BRC4 peptides and subjected to immunoprecipitation (IP) using anti-GFP affinity resin. Inputs and co-immunoprecipitated protein complexes were analyzed by immunoblotting.

Figure 2. The cell-penetrating peptide nona-arginine (R9) mediates efficient delivery of BRC4 peptides into human cells.

A, HeLa and U2OS cells were stained for 30 minutes with Hoechst 33342 to visualize nuclei and washed with PBS before adding 10 µM of the indicated TAMRA-labeled peptides. After 1-hour incubation in serum-free medium, cells were washed thoroughly to remove any membrane-bound peptides and live cells were directly

Downloaded from mct.aacrjournals.org on May 23, 2018. © 2018 American Association for Cancer Research.

Author Manuscript Published OnlineFirst on April 13, 2018; DOI: 10.1158/1535-7163.MCT-17-1156
Author manuscripts have been peer reviewed and accepted for publication but have not yet been edited.

imaged on a confocal microscope. Gains were adjusted for each condition to reduce background fluorescence and to visualize strong and weak signals at the same time. The scale bar represents 20 μm. **B,** HeLa and U2OS cells were transfected with 10 μM of the indicated TAMRA-labeled peptides in serum-free medium for 1 hour. Cells were harvested by trypsinization and TAMRA signal intensities were recorded on a flow cytometer by scoring 20'000 events. Bar graph depicts median TAMRA fluorescence intensity. a.u. = arbitrary units. Data are presented as the mean ± s.d. (n = 3). **C,** HeLa and U2OS cells were incubated with 10 μM of the indicated TAMRA-labeled peptides. After 1 hour, cells were harvested by trypsinization. 10 pmol of freshly solubilized peptides (lanes 2-5) and whole-cell lysates of 70'000 peptide-transfected cells (lanes 6-15) were loaded onto Tricine SDS-PAGE gel and TAMRA signals were visualized using a FluoroImager.

Figure 3. R9-BRC4 peptides have an approximate half-life of 2-4 hours upon cell entry.

A, HeLa cells were transfected with 10 μM of the indicated Fluorescein-labeled peptides in serum-free DMEM for 1 hour, followed by a release in serum-containing medium for the indicated time points. Left panel, 10 pmol of freshly solubilized peptides (lane 2) and whole-cell lysates of peptide-transduced cells (lanes 3-7) were loaded onto Tricine SDS-PAGE gel and Fluorescein signals were analyzed using a FluoroImager. Right panel, quantification of relative Fluorescein signal intensities of intact full-length R9-BRC4^{wt} and R9-BRC4^{mut} peptides. Data are represented as mean ± s.d. (n = 4). **B,** HeLa cells incubated with Fluorescein-R9-BRC^{wt} peptides as in (A) were analyzed by flow cytometry recording 20'000 events for each condition. The

Downloaded from mct.aacrjournals.org on May 23, 2018. © 2018 American Association for Cancer Research.

Author Manuscript Published OnlineFirst on April 13, 2018; DOI: 10.1158/1535-7163.MCT-17-1156
Author manuscripts have been peer reviewed and accepted for publication but have not yet been edited.

intensity of the Fluorescein signal is plotted against the side-scatter area (SSC-A). Gates display percentages of cells showing moderate to high fluorescent intensities.

Figure 4. BRC4 peptide inhibits RAD51 foci formation and homologous recombination.

A, HeLa cells were either transfected with control (CNTL) or BRCA2 siRNA oligos for 48 hours, or incubated with 10 μM of the indicated cell-penetrating peptides (CPPs) for 1 hour before treatment with 100 nM camptothecin (CPT) for 1 hour. Whole-cell lysates were analyzed by immunoblotting using the indicated antibodies. **B** and **C,** Same cells as in (A) were treated with 100 nM CPT for 1 hour before transfecting them with the depicted peptides (10 μM) for 1 hour and releasing them for 3 hours in serum-containing medium. Cells were pre-extracted, fixed, and immunostained for RAD51. (B) Scale bars represent 10 μm and 5 μm (Zoom). (C) The graph illustrates the percentage of cells displaying more than 10 RAD51 foci/nucleus. For each condition at least 100 cells were scored. **D,** Same cells as in (A) were irradiated with increasing doses of IR, peptide-transfected (10 μM) and released for 3 hours in serum-containing medium prior to pre-extraction, fixation, and immunostaining for RAD51. The graph illustrates the percentage of cells displaying more than 10 RAD51 foci/nucleus. For each condition at least 100 cells were scored. **E,** HeLa DR-GFP cells were transfected with the *I-SceI* expression plasmid 48 hours post-siRNA transfection. Alternatively, one-hour incubation periods with 10 μM peptides took place 4 hours, 24 hours and 34 hours post-*I-SceI* transfection of HeLa DR-GFP cells. A second siRNA transfection was performed 24 hours after I-SceI transfection. Cells were harvested 48 hours post-*I-SceI* transfection and GFP-positive cells were scored by flow cytometry. 20'000 events were recorded. The graph

Downloaded from mct.aacrjournals.org on May 23, 2018. © 2018 American Association for Cancer Research.

Author Manuscript Published OnlineFirst on April 13, 2018; DOI: 10.1158/1535-7163.MCT-17-1156
Author manuscripts have been peer reviewed and accepted for publication but have not yet been edited.

illustrates the percentage of GFP-positive cells as a read-out for HR efficiency. Data in **C, D** and **E** display the mean ± s.d. ($n \geq 3$). Statistical significance (***, p-value ≤ 0.001; ns, non significant) was calculated with Tukey's multiple comparison test using two-way ANOVA (C and D) and one-way ANOVA (E).

Figure 5. BRC4 peptide provokes MRE11-dependent degradation of stalled DNA replication forks.

A, U2OS cells were transfected with indicated siRNA oligos for 48 hours or left untransfected. Subsequently, cells were labeled with CIdU and IdU before adding hydroxyurea (HU) together with indicated peptides (10 μM) in serum-free medium for 4 hours followed by DNA fiber spreading. Upper panel shows the experimental set up, representative DNA fiber images and their corresponding IdU/CIdU ratios, respectively. Lower panel shows IdU/CIdU ratios for each condition illustrated by a dot plot with mean ratios denoted as a red line. **B,** Same cells as in (A) were additionally treated with the MRE11 inhibitor mirin. **C,** U2OS cells were transfected with the indicated siRNA oligos for 48 hours before dual labeling and HU treatment in combination with 10 μM R9 or R9-BRC4^{wt} peptides. Representative immunblot is shown to indicate individual knockdown efficiencies. Approximately 250 DNA replication tracks were scored and numbers indicate the mean ± s.d. ($n = 2$). Statistical differences (****, p-value ≤ 0.0001; ns, non significant) were determined by Mann-Whitney U test.

Figure 6. BRC4 peptide sensitizes cancer cells to PARP inhibition.

A, HeLa cells were transfected with the indicated siRNAs or left untransfected for standard peptide transduction. 24 hours later, cells were plated at low cell density into

Downloaded from mct.aacrjournals.org on May 23, 2018. © 2018 American Association for Cancer Research.

Author Manuscript Published OnlineFirst on April 13, 2018; DOI: 10.1158/1535-7163.MCT-17-1156
Author manuscripts have been peer reviewed and accepted for publication but have not yet been edited.

24-well plates. Another 24 hours later, non-siRNA transfected cells were incubated for 1 hour with 10 μM of peptides in serum-free medium supplemented with 1 μM olaparib. Finally, serum-containing medium supplemented with 1 μM olaparib was added, cells were grown for 10 days and colonies were stained using crystal violet. Representative images of a colony formation assay are shown. Clonogenic survival was determined by quantifying the colony intensity of olaparib-treated relative to untreated and is depicted as bar graph. Data are represented as mean ± s.d. (n = 4). Statistical significance (***, p-value ≤ 0.001; ns, non significant) was calculated with Tukey's multiple comparison test using one-way ANOVA. **B,** Peptide-transfected HeLa cells as in (A) were treated with increasing concentrations of olaparib and survival was determined by colony formation assay. **C,** Same cells as in (A) were treated with 1 μM olaparib in combination with increasing concentrations of BRC4 peptides and survival was determined by colony formation assay. **D,** Same cells as in (B) were treated with 10 μM of the RAD51 inhibitor BO2 under identical experimental conditions as used for the BRC4 peptide and survival was determined by colony formation assay. Data in **B-D** are represented as mean ± s.d. (n ≤ 3). **E,** HeLa, U2OS, RPE1, MRC5 and MCF10A were identically treated as in (A) and survival was determined by colony formation assay. Left panel, knockdown efficiencies were analyzed by immunoblotting of whole-cell lysates of indicated cell lines. Right panel, relative clonogenic survival is depicted as mean ± s.d. (n = 4). Statistical significance (****, p-value ≤ 0.0001; **, p-value ≤ 0.01; ns, non significant) was calculated with Tukey's multiple comparison test using one-way ANOVA.

Downloaded from mct.aacrjournals.org on May 23, 2018. © 2018 American Association for Cancer Research.

Author Manuscript Published OnlineFirst on April 13, 2018; DOI: 10.1158/1535-7163.MCT-17-1156
Author manuscripts have been peer reviewed and accepted for publication but have not yet been edited.

Figure 1

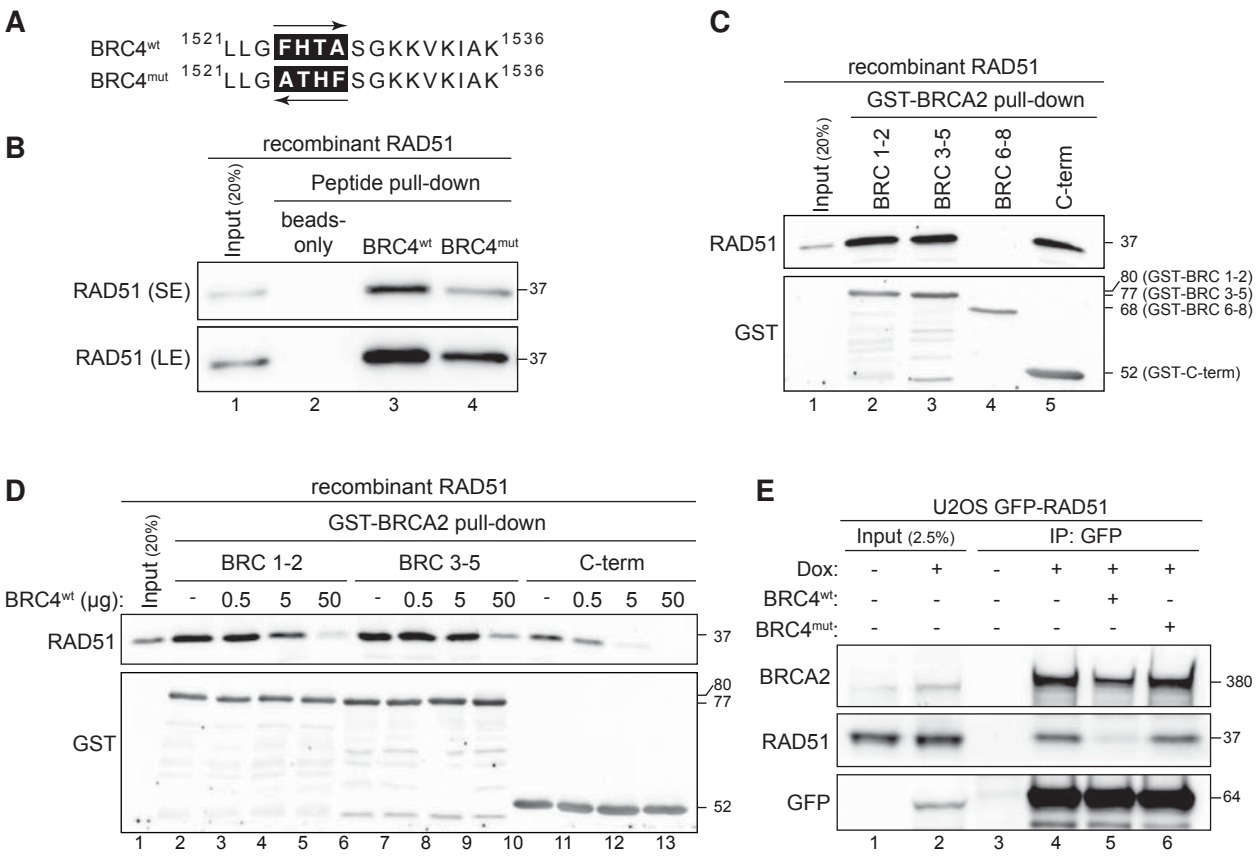

Downloaded from mct.aacrjournals.org on May 23, 2018. © 2018 American Association for Cancer Research.

Author Manuscript Published OnlineFirst on April 13, 2018; DOI: 10.1158/1535-7163.MCT-17-1156
Author manuscripts have been peer reviewed and accepted for publication but have not yet been edited.

Figure 2

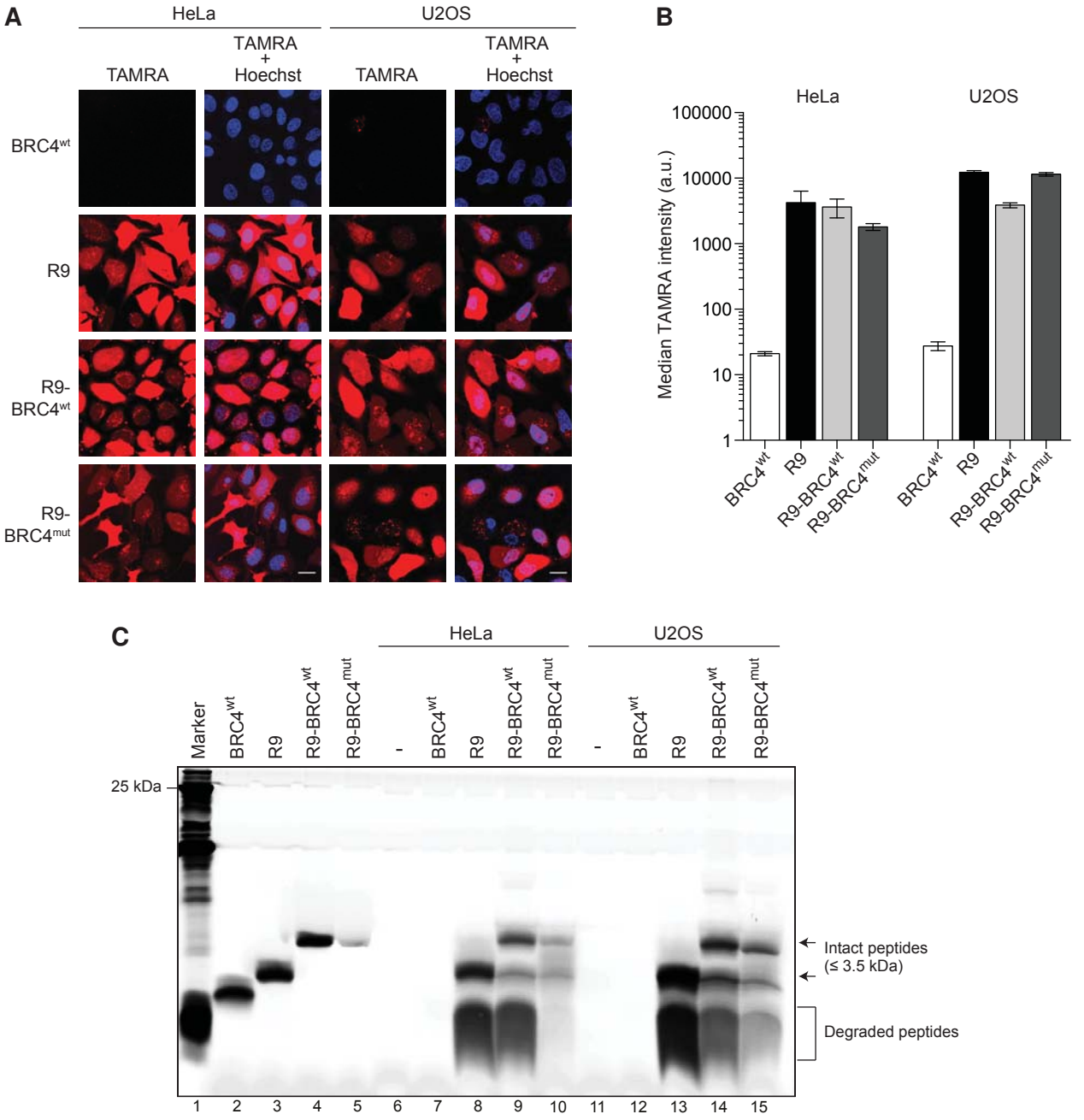

Downloaded from mct.aacrjournals.org on May 23, 2018. © 2018 American Association for Cancer Research.

Author Manuscript Published OnlineFirst on April 13, 2018; DOI: 10.1158/1535-7163.MCT-17-1156
Author manuscripts have been peer reviewed and accepted for publication but have not yet been edited.

Figure 3

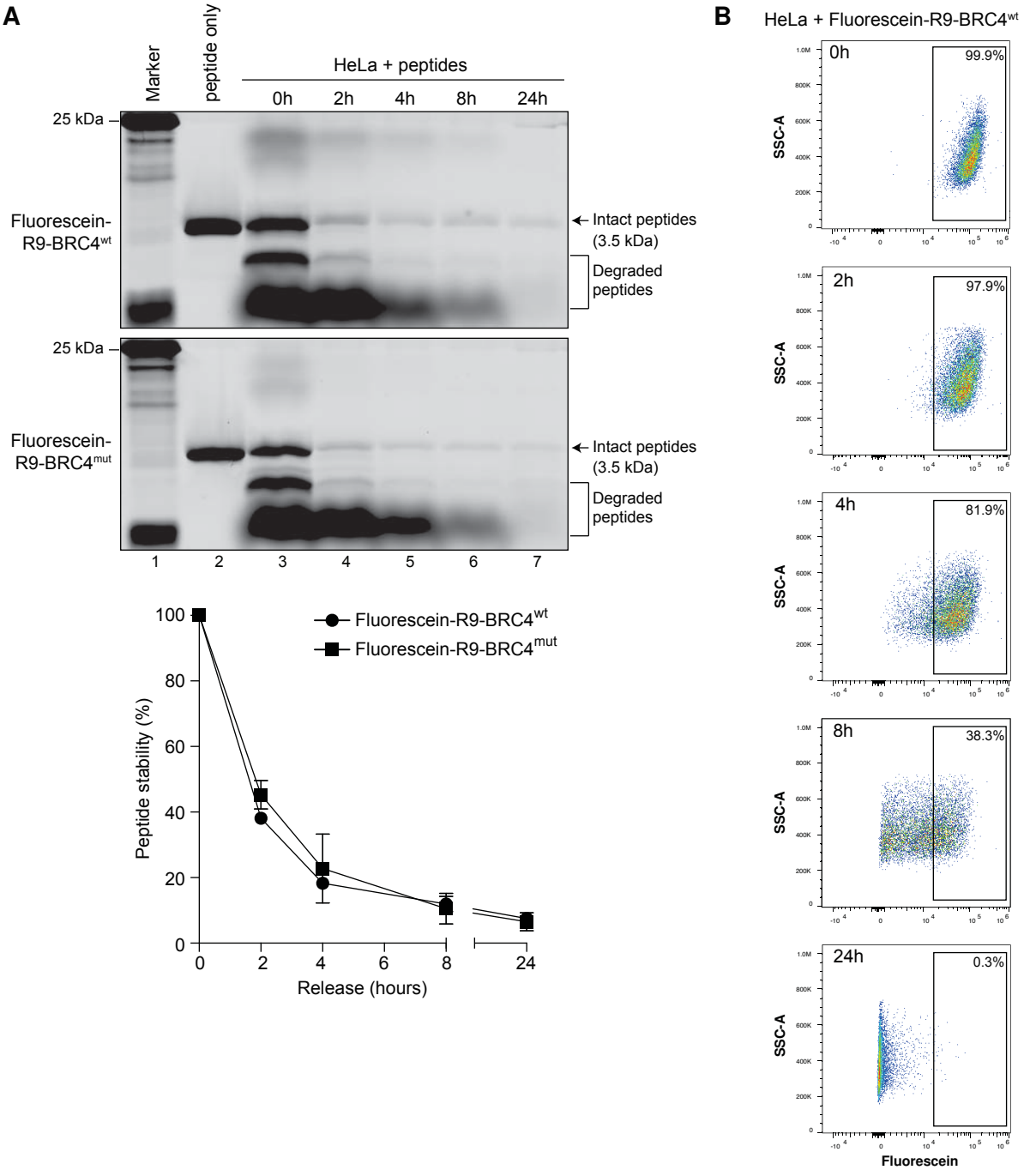

Downloaded from mct.aacrjournals.org on May 23, 2018. © 2018 American Association for Cancer Research.

Author Manuscript Published OnlineFirst on April 13, 2018; DOI: 10.1158/1535-7163.MCT-17-1156
Author manuscripts have been peer reviewed and accepted for publication but have not yet been edited.

Figure 4

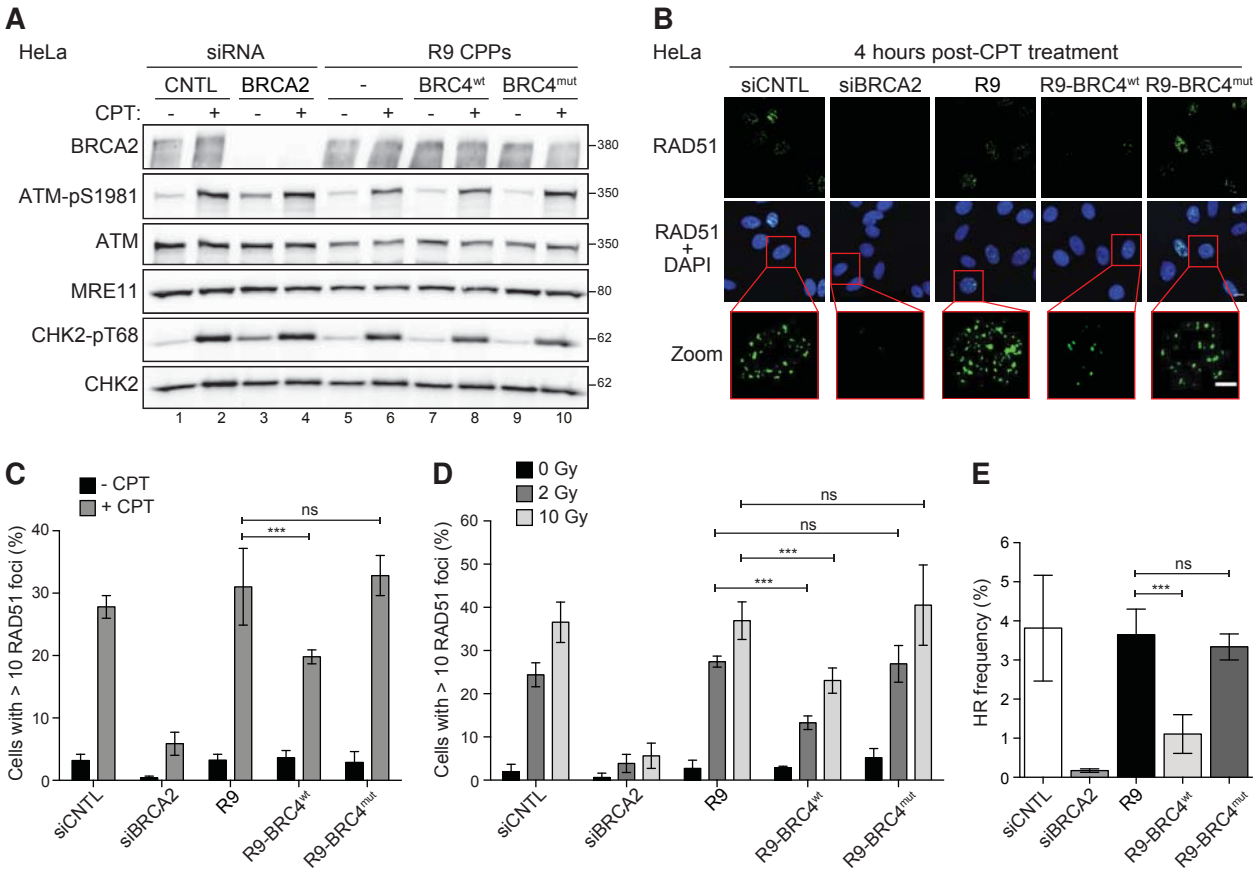

Downloaded from mct.aacrjournals.org on May 23, 2018. © 2018 American Association for Cancer Research.

Author Manuscript Published OnlineFirst on April 13, 2018; DOI: 10.1158/1535-7163.MCT-17-1156
Author manuscripts have been peer reviewed and accepted for publication but have not yet been edited.

Figure 5

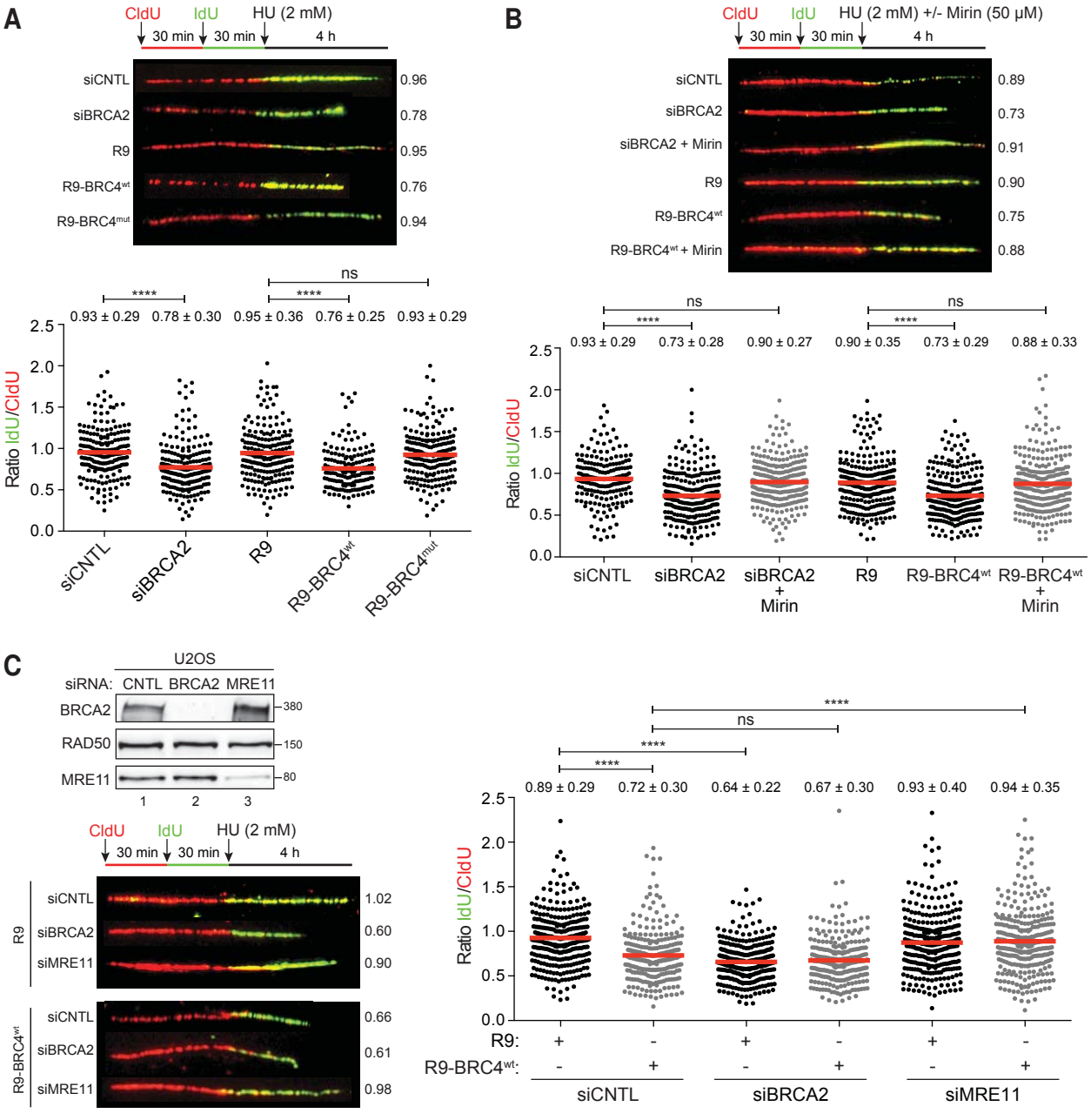

Downloaded from mct.aacrjournals.org on May 23, 2018. © 2018 American Association for Cancer Research.

Author Manuscript Published OnlineFirst on April 13, 2018; DOI: 10.1158/1535-7163.MCT-17-1156
Author manuscripts have been peer reviewed and accepted for publication but have not yet been edited.

Figure 6

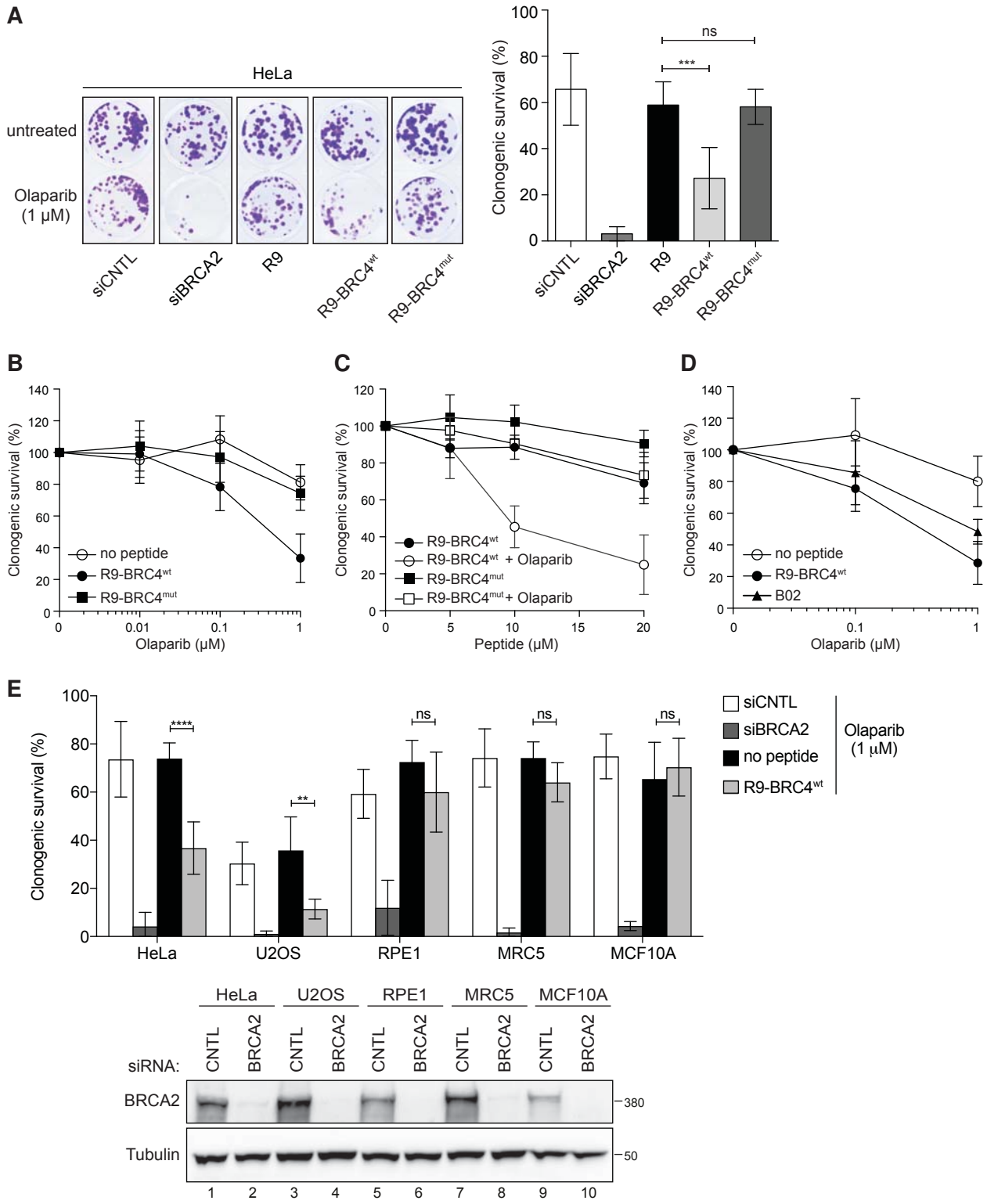

Downloaded from mct.aacrjournals.org on May 23, 2018. © 2018 American Association for Cancer Research.

Author Manuscript Published OnlineFirst on April 13, 2018; DOI: 10.1158/1535-7163.MCT-17-1156
Author manuscripts have been peer reviewed and accepted for publication but have not yet been edited.

AACR American Association for Cancer Research

Molecular Cancer Therapeutics

A short BRCA2-derived cell-penetrating peptide targets RAD51 function and confers hypersensitivity towards PARP inhibition

Anika Trenner, Julia Godau and Alessandro A Sartori

Mol Cancer Ther Published OnlineFirst April 13, 2018.

Updated version	Access the most recent version of this article at: doi:10.1158/1535-7163.MCT-17-1156
Supplementary Material	Access the most recent supplemental material at: http://mct.aacrjournals.org/content/suppl/2018/04/13/1535-7163.MCT-17-1156.DC1
Author Manuscript	Author manuscripts have been peer reviewed and accepted for publication but have not yet been edited.

E-mail alerts	Sign up to receive free email-alerts related to this article or journal.
Reprints and Subscriptions	To order reprints of this article or to subscribe to the journal, contact the AACR Publications Department at pubs@aacr.org.
Permissions	To request permission to re-use all or part of this article, use this link http://mct.aacrjournals.org/content/early/2018/04/13/1535-7163.MCT-17-1156. Click on "Request Permissions" which will take you to the Copyright Clearance Center's (CCC) Rightslink site.

Downloaded from mct.aacrjournals.org on May 23, 2018. © 2018 American Association for Cancer Research.